LANGMUIR

pubs.acs.org/Langmuir Article

Water-Stable 1D Double-Chain Cu Metal–Organic Framework-based Electrochemical Biosensor for Detecting L-Tyrosine

Xiao-Qin Wu,* Pei-Qi Feng, Zhiqiang Guo, and Xuehong Wei

Cite This: https://dx.doi.org/10.1021/acs.langmuir.0c02799 Read Online

ACCESS | Metrics & More | Article Recommendations | Supporting Information

ABSTRACT: An electrochemical biosensor based on a water-stable one-dimensional double-chain Cu(II) metal–organic framework (Cu-MOF) directly was constructed for efficiently recognizing L-tyrosine (L-Tyr) in biomimic environments. Cu-MOF: $\{[Cu(bpe)(fdc)(H_2O)(DMF)]\cdot 0.5H_2O\}_n$ (bpe = 1,2-di(4-pyridyl)ethylene, H_2fdc = 2,5-furandicarboxylic acid, namely, **Cu-1**) was synthesized by a hydrothermal method. It was characterized by IR, scanning electron microscopy, atomic force microscopy, and PXRD techniques. **Cu-1** exhibited extreme solvent and thermal stability as well as excellent electroconductive character. It was coated on a glassy carbon electrode (GCE) surface to prepare an electrochemical biosensor (**Cu-1**/GCE) which showed preferable biosensing ability toward L-Tyr. This Cu-MOF electrochemical biosensor showed simple operation and high sensitivity toward L-Tyr in the concentration range from 0.01 to 0.09 mM. The detection limit is 5.822 μM. Furthermore, **Cu-1**/GCE showed extremely excellent selectivity to L-Tyr in a biomimic environment with several amino acid interferents. This new strategy exhibits great potential applications for designing MOFs with excellent electrochemical activity.

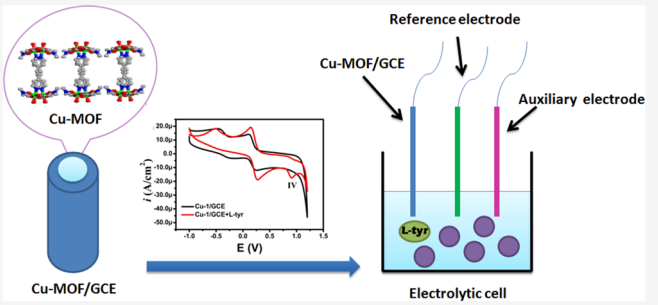

INTRODUCTION

Amino acids are a kind of biochemical reagents with chemical active properties; they are not only important biomarkers for various metabolic diseases but also safe corrosion inhibitors for metallic alloy materials.[1,2] As a member of the amino acid family, tyrosine is a conditionally essential amino acid and an important raw material in cosmetics and medicine fields.[3−7] Various techniques[8−16] have been explored for small biomolecule tyrosine recognizing. The chemical sensor technology is based on the combination of both molecular recognition and sensing technology by a specific receptor to get information of the guest molecules and then through the corresponding signal transduction mechanism combines the molecule information into electrochemical signals so as to realize real-time detecting guest molecules in situ. The preparation of the molecular recognition receptor is key to the chemical sensor technology. Traditional receptor substrate materials mainly focus on organic polymers,[17,18] carbon materials,[19−21] metal nanoparticles,[22,23] and other electrochemical activity composites[24,25] for their excellent electrical conductivity.

In recent years, metal–organic frameworks (MOFs) as inorganic–organic hybrid multifunctional materials with many amazing features, such as a changeable skeleton structure, adjustable pore sizes, and exposed metal activity sites, attracted many attentions in the chemical sensor field.[26−28] There are many groups who attempted to explore MOFs as template composites with other electrochemical active substances for preparing receptors of the chemical sensor.[29−33] These strategies mostly use simple doped methods or post-modification ways, and MOFs always play a role in the synergistic effect to promote electroconductive ability. However, few MOFs directly applied as electrochemical sensor materials are reported. The reason is that most of them showed solvent and air instability as well as low electroconductivity. Thus, how to design MOFs suitable for sensor materials is still a challenge for researchers.

In this paper, we first synthesized a water-stable Cu-MOF: $\{[Cu(fdc)(bpe)(H_2O)(DMF)]\cdot 0.5H_2O\}_n$ (bpe = 1,2-di(4-pyridyl)ethylene, H_2fdc = 2,5-furandicarboxylic acid, namely, **Cu-1**) by a hydrothermal method. Because of its excellent solvent stability and electrical conductivity, **Cu-1** as a sensor material without postmodification was coated on a glassy carbon electrode (GCE) surface to prepare **Cu-1**/GCE. This modified electrode was used as an electrochemical biosensor for detecting L-tyrosine (L-Tyr) in biomimic environments (Scheme 1). **Cu-1** as an MOF material provided naked activity sites and well-organized frameworks which can selectively

Received: September 23, 2020
Revised: October 30, 2020

Scheme 1. Schematic Illustration of the Preparation, Modification, and Analytical Procedure of Cu-1/GCE for the Determination of L-Tyr

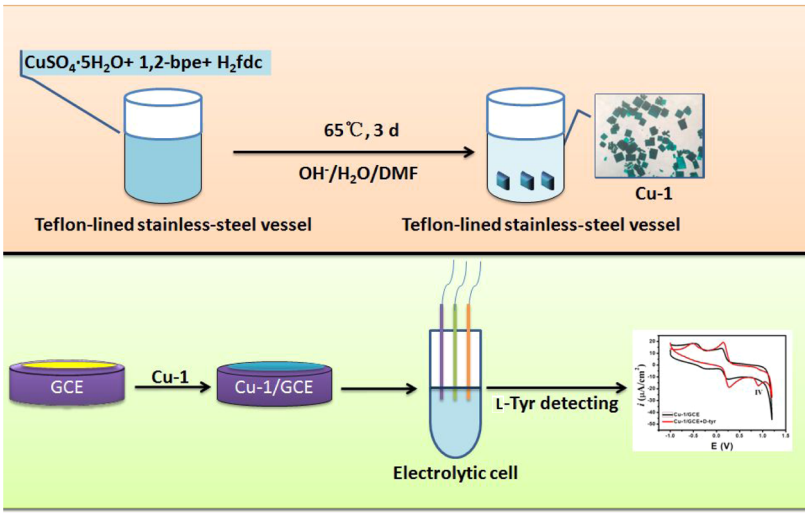

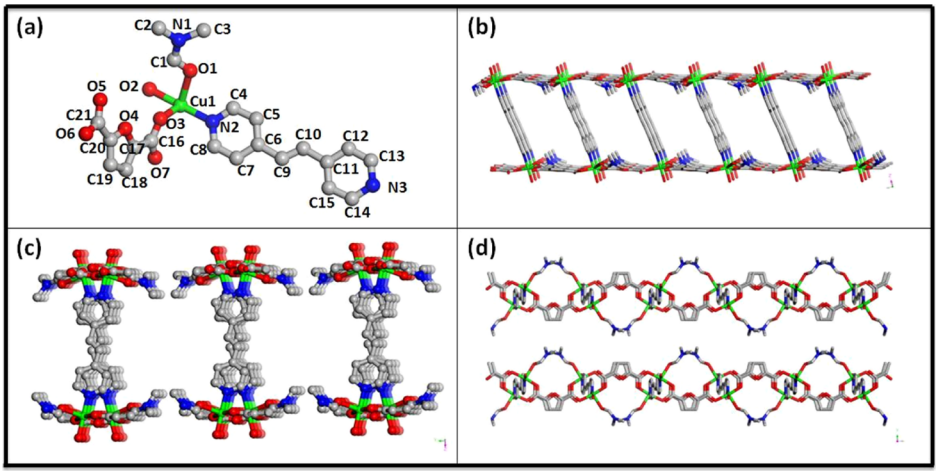

Figure 1. (a) Asymmetric unit of **Cu-1**; (b) 1D double-stranded structure seen in a plane extending the *X*- and *Z*-axes of **Cu-1**; (c) structure of **Cu-1** along the *X*-axes; (d) structure of **Cu-1** along the *Z*-axes.

recognize the small biomolecule L-Tyr. The aim of this work is to provide a method for designing MOFs which have electrochemical activity and are suitable to electrochemical biosensor materials to specifically detect small biological molecules. This work has the following advantages: (i) design and synthesis of MOFs with good electroconductivity and excellent solvent and air stability properties, (ii) simple assembly of electrochemical biosensors through direct usage of MOFs without postmodification, (iii) efficient sensing performances with high sensitivity and excellent selectivity caused by the molecular recognition between the Cu(II) MOF (Cu-MOF) and small biological molecules, and (iv) broadening of the MOF application in the electrochemical biosensor technology.

EXPERIMENTS

Materials and Instruments. Cupric(II) sulfate ($CuSO_4·5H_2O$, 99%), 2,5-furandicarboxylic acid (fdc, >99%), 1,2-di(4-pyridyl)-ethylene (bpe, >99%), *N*,*N*-dimethylformamide (DMF, >99%), sodium hydroxide (NaOH, >99%), and L-tyrosine (L-Tyr, 99%) and other amino acids were purchased from commercial suppliers (Aladdin Reagent and J&K Reagent). Ultrapure water was used as a solvent for preparing the solutions. The ultrasonic process was handled with an ultrasonic cleaning machine (Elma, S100H). The crystal data of **Cu-1** were collected using a Bruke D8 Venture X-ray single-crystal diffractometer. A NETZSCH TG 209 instrument was used to perform thermogravimetric analysis (TGA) experiments with a heating rate of 10 °C min^{-1}. A D/Max-2500 X-ray diffractometer was used for analyzing the phase purity of **Cu-1**. A Bruker Tensor 27 spectrophotometer was used for measuring the FT-IR spectra. A Chi660e electrochemical workstation (Chenhua, China) was used for all the electrochemical studies.

Synthesis of {[Cu(bpe)(fdc)(H_2O)(DMF)]·0.5H_2O}$_n$·(Cu-1). A mixture containing $CuSO_4·5H_2O$ (49.94 mg, 0.2 mmol), 1,2-bpe (3.644 mg, 0.02 mmol), fdc (6.244 mg, 0.04 mmol), NaOH (≥98.0%, 1.6 mg) water (4 mL), and DMF (4 mL) was sealed in a Teflon-lined stainless-steel vessel (23 mL). This vessel was heated at 65 °C for 3 days and subsequently cooled to room temperature. Blue stick crystals of **Cu-1** were obtained in the bottom of the vessel, collected, washed with ultrapure water, and dried in air. The yield of **Cu-1** was 16.6 mg (27.02%).

Fabrication of Cu-1/GCE. Prior to be used, the GCE (Φ = 3 mm) was cleaned with Al_2O_3 powder (sizes: 0.03 and 0.05 μm, respectively) to remove residual substance and then washed using ethanol and double-distilled water with an ultrasonic cleaner successively. The pretreated electrode was immersed in deionized water for later use. **Cu-1** (1 mg) was dispersed in 1 mL of Nafion

https://dx.doi.org/10.1021/acs.langmuir.0c02799
Langmuir XXXX, XXX, XXX−XXX

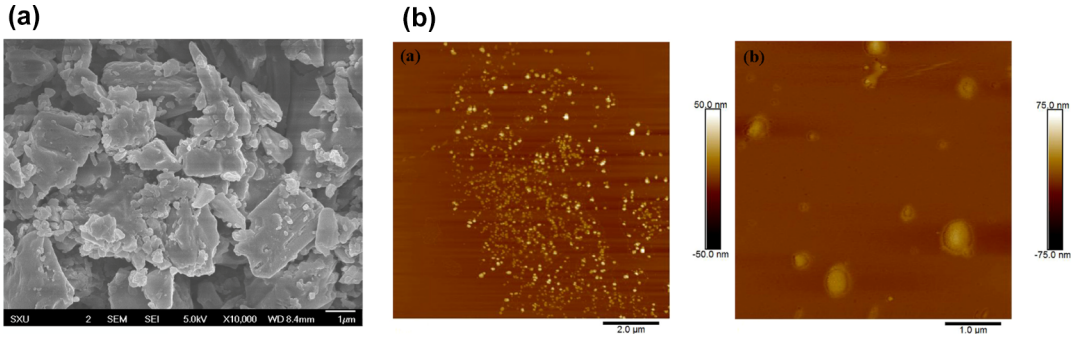

Figure 2. (a) SEM image and (b) AFM images of **Cu-1**, denoted as (a) and (b) within the image.

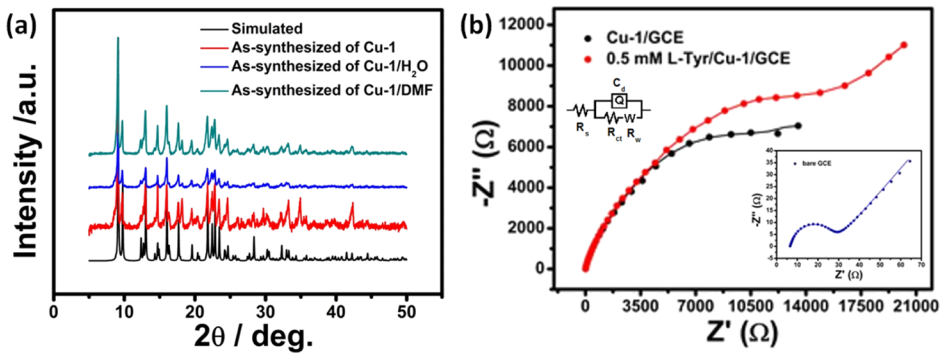

Figure 3. (a) PXRD graphs of **Cu-1**: the simulated one from single-crystal data, the one as synthesized, and the one after immersing in water or the DMF solvent for 1 week. (b) Nyquist plots of impedance spectra at the bare GCE, **Cu-1**/GCE, and 0.5 mM L-Tyr/**Cu-1**/GCE.

solution under sonication for 5 min and let stand for more than 3 h. Next, 8 μL of this solution was coated on the GCE electrode surface and dried under ambient conditions for one night. Thus, the **Cu-1**-modified GCE (**Cu-1**/GCE) was obtained. When not in use, **Cu-1**/GCE was stored at 4 °C in a refrigerator.

Electrochemical Measurements. A three-electrode system was used for all electrochemical experiments. It consists of a bare GCE or **Cu-1**/GCE as the working electrode, a saturated calomel electrode as the reference electrode, and a platinum wire as the counter electrode. Electrochemical impedance spectroscopy (EIS) was performed using the abovementioned three-electrode system. EIS was performed in 1 mM KCl containing 0.1 mM $[Fe(SCN)_6]^{4-/3-}$ solution with a frequency range of 0.1 Hz to 100 kHz with an open-circuit potential of 0.19 V. All studies were carried out at room temperature and under nitrogen surroundings.

RESULTS AND DISCUSSION

Characterization of Cu-1. In this work, a one-dimensional (1D) Cu-MOF with a formula of $\{[Cu(bpe)(fdc)(H_2O)\cdot(DMF)]\cdot 0.5H_2O\}_n$ (**Cu-1**, bpe = 1,2-di(4-pyridyl)ethylene, H_2fdc = 2,5-furandicarboxylic acid) was designed and synthesized by a hydrothermal method. Single-crystal X-ray diffraction data reveal that **Cu-1** crystallizes in the monoclinic space group *C*2/*c*. The asymmetric unit consists of a pentacoordinated Cu^{2+} ion, two fdc^{2-} ligands, one bpe ligand, one DMF, and one H_2O molecule. **Cu-1** is pentacoordinated by four O atoms (from two fdc^{2-} ligands, one DMF, and one H_2O molecule) and one N atom (from the bpe ligand) (Figure 1a). This asymmetric unit further extended along the *y*-axis by the ligands fdc^2 to afford a 1D chain. Moreover, two 1D chains are connected by another N atom of the bpe ligand to form a 1D double-stranded structure (Figure 1b). **Cu-1** presents different shapes along different axes (Figure 1c,d).

The morphology study of **Cu-1** was performed by scanning electron microscopy (SEM) and atomic force microscopy (AFM). **Cu-1** presented a blocklike structure, while the AFM figure of **Cu-1** with a rough surface presented a granular structure (Figure 2). After immersion in water or the DMF solvent for at least 1 week, the PXRD patterns reveal that these crystals of **Cu-1** can still be conformed with the simulated one from the single-crystal data (Figure 3a), which indicated that **Cu-1** exhibits excellent phase purity and solvent stability.

EIS Studies. EIS was used to investigate the surface features of the bare GCE and **Cu-1**/GCE at each detection step. The Nyquist plots of EIS were recorded from 0.1 Hz to 100 kHz at 0.19 V in a solution containing 0.1 mM KCl and 0.1 mM $[Fe(SCN)_6]^{4-/3-}$ (Figure 3b).

The typical impedance spectroscopy was composed of two parts: a semicircle portion at high frequencies representing the charge-transfer resistance (R_{ct}) and a linear part at low frequencies corresponding to the diffusion process.[34] The R_{ct} value represented the charge-transfer kinetics of the $[Fe(SCN)_6]^{4-/3-}$ redox system. The bare GCE exhibited a small resistance with a R_{ct} value of 301.4 μΩ·cm^2. Also, the R_{ct} value of **Cu-1**/GCE was 16.9 mΩ·cm^2; the significantly increasing R_{ct} value was attributed to the reduced electroconductivity after coating the Cu-MOF and caused the reduced electron transfer. This phenomenon showed that **Cu-1** was successfully modified onto the GCE surface. After adding 0.5 mM L-Tyr to the electrolyte system, the R_{ct} value of **Cu-1**/GCE increased to 29.1 mΩ·cm^2. The gradually increased impedance suggested that the highly specific recognition hindered the electroconductivity and L-Tyr can be detected by the **Cu-1**/GCE electrochemical sensor.

Cyclic Voltammetry Behavior Studies. As a good electroactive substance, potassium ferricyanide is often used to study electron transfer in biosensors, solar cells, and other systems.[35,36] As known, the electrochemical behavior of the

https://dx.doi.org/10.1021/acs.langmuir.0c02799
Langmuir XXXX, XXX, XXX−XXX

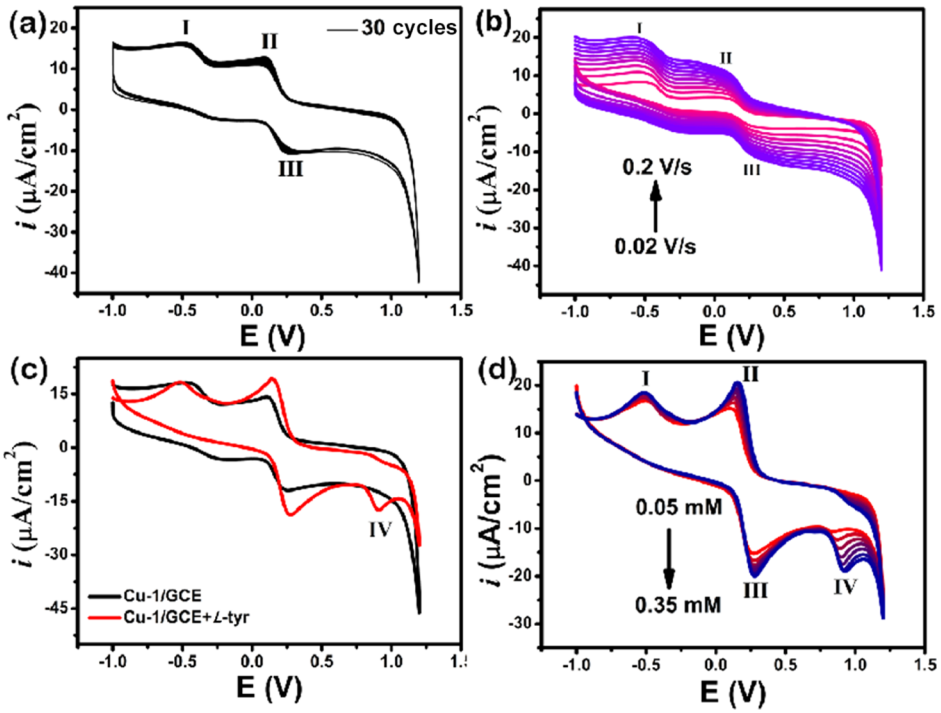

Figure 4. (a) Cyclic voltammograms at **Cu-1**/GCE for 30 cycles. (b) Cyclic voltammograms at **Cu-1**/GCE with different scan rates in the range of 0.02−0.2 V·s^{-1}. (c) Cyclic voltammograms at **Cu-1**/GCE (black) and after adding 0.5 mM L-Tyr (red). (d) Cyclic voltammograms at **Cu-1**/GCE with L-Tyr concentrations of 0.05, 0.1, 0.15, 0.2, 0.25, 0.3, and 0.35 mM. Scan rate: 50 mV·s^{-1}. Electrolyte: 1 mM KCl containing 0.1 mM $[Fe(SCN)_6]^{4-/3-}$ solution.

potassium ferricanocyanide $[Fe(SCN)_6]^{4-/3-}$system in neutral aqueous solutions is a reversible process. The oxidation peak and reduction peak of oxygen are symmetrical, and the current value of the two peaks is almost the same. The theoretical value of peak−peak potential difference is 59 mV at the bare electrode. Thus, cyclic voltammetry (CV) of **Cu-1**/GCE was carried out in the $[Fe(SCN)_6]^{4-/3-}$system for 30 cycles to characterize its electrochemical stability.

As can be seen in Figure 4a, in addition to the redox characteristic peaks II and III in the potassium ferricyanide system, another obvious oxidation peak I at −0.48 V belonged to **Cu-1** and its current density nearly did not decrease after 30 cycles. It showed good reproducibility which originated from the excellent electrochemical stability of **Cu-1**. The influences of scan rates (ν) were also studied. The cyclic voltammograms of **Cu-1**/GCE in 1 mM KCl containing 0.1 mM $[Fe(SCN)_6]^{4-/3-}$ solution with a scan rate range of 0.02−0.2 V s^{-1} are shown in Figure 4b. Both the oxidation and reduction process peak current densities increased gradually with the increasing scan rates. The electrochemical active surface area (ECSA) of **Cu-1**/GCE was calculated as 1.242 cm^2 according to the Randles−Sevcik equation:[37] $i_p = 268{,}600n^{2/3}AD^{1/2}C\nu^{1/2}$, where i_p is the peak I current density (A·cm^{-2}), n is the number of electrons transferred (n = 1), A is the ECSA (cm^2), D is the diffusion coefficient in cm^2/s (6.70×10^{-6} cm^2/s), C is the concentration in mol/L (0.005 M $K_3Fe(CN)_6$), and ν is the scan rate (V·s^{-1}). It indicated that **Cu-1** has a large ECSA and shows high electrochemical stability and reproducibility. The results showed that **Cu-1** has an excellent sensing property and it is suitable for electrochemical biosensor materials.

Tyrosine as a member of the amino acid family can be used as an amino acid with few side effects to treat diseases such as tuberculosis encephalitis and polio. It can promote the formation of melanin, which is essential for the treatment of vitiligo. In whitening cosmetics, tyrosine is a significant additive in the production of eumelanin and pheomelanin.[38,39] Therefore, the study of tyrosine is very important in the clinical diagnosis and cosmetics industry. First, the electrochemical behavior of L-Tyr at the bare GCE was studied. No obvious electrochemical signals were observed when 0.25 mM L-Tyr was added to the electrolyte (Figure S5). It indicated that the electrocatalytic recognizing effect of the bare GCE toward L-Tyr was almost inconspicuous.

Subsequently, **Cu-1**/GCE was used as a sensor for detecting L-Tyr. CV was performed on **Cu-1**/GCE in the $[Fe(SCN)_6]^{4-/3-}$ system with the presence of 0.25 mM L-Tyr (Figure 4c). Compared with the blank one (black curve), oxidation peak I ($E_{p,I}$ = −0.48 V) belonging to **Cu-1** can still be observed; $[Fe(SCN)_6]^{4-/3-}$ characteristic peaks II and III ($E_{p,II}$ = 0.076 V, $E_{p,III}$ = 0.176 V) slightly shifted to ±0.5 mV because of mass-transfer delay in the L-Tyr detecting CV curves. Furthermore, a sharp and distinct L-Tyr detecting signal can be observed at a more positive potential of $E_{p,IV}$ = 0.91 V with an $i_{p,IV}$ value of −17.5 μA·cm^{-2}.

The mechanisms of the interaction between L-Tyr and **Cu-1** might be due to three factors: first, because of the electrochemical interaction, L-Tyr was absorbed into the nearby **Cu-1** skeleton; second, there are many coordinated water molecules which in ordered rows in the **Cu-1** framework, and these active O atoms can interact with $-NH_2$ from the guest molecule L-Tyr by van der Waals interactions or hydrogen bond interactions; third, **Cu-1** provides a suitable spatial effect and a sufficient surface area to recognize L-Tyr molecules. The huge surface area and the orderly pore structure of **Cu-1** promise its probability for absorbing ability.

https://dx.doi.org/10.1021/acs.langmuir.0c02799
Langmuir XXXX, XXX, XXX−XXX

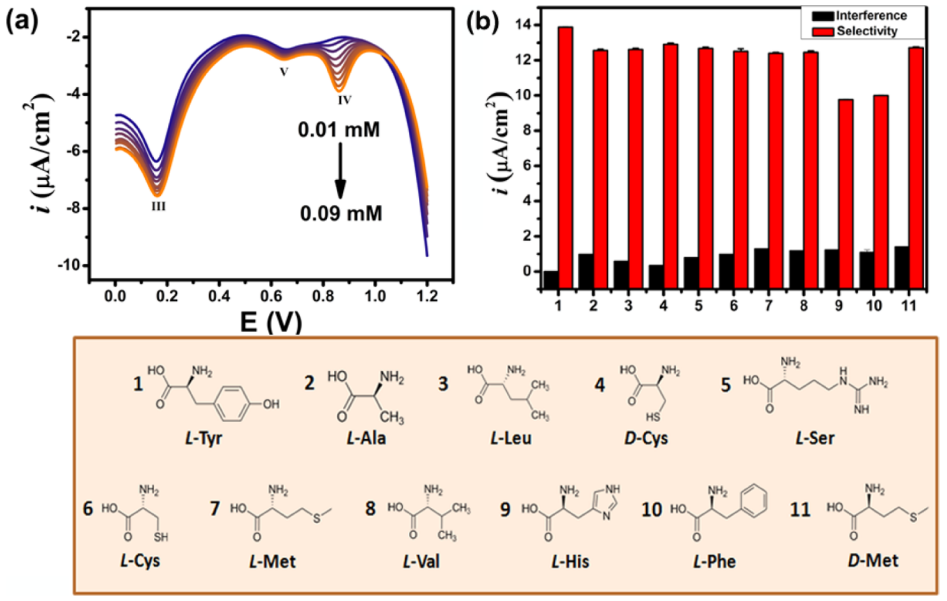

Figure 5. (a) Differential pulse voltammograms of various concentrations of L-Tyr 0.01, 0.02, 0.03, 0.04, 0.05, 0.06, 0.07, 0.08, and 0.09 mM on **Cu-1**/GCE in 1 mM KCl containing 0.1 mM $[Fe(SCN)_6]^{4-/3-}$ solution. (b) Selectivity and interference tests of **Cu-1**/GCE; the concentrations of the interferents L-alnine (L-Ala), L-leucine (L-Leu), D-cysteine (D-Cys), L-serine (L-Ser), L-cysteine (L-Cys), L-methionine (L-Met), L-valine (L-Val), L-histidine (L-His), L-phenylalanine (L-Phe), and D-methionine (D-Met) were 0.1 mM.

The concentration influences of L-Tyr were investigated. The peak IV current density increased gradually with the increase of L-Tyr concentration in the range from 0.05 to 0.35 mM (Figure 4d). The linear variation equation of $i_{p,IV}$ versus the L-Tyr concentration was given as follows (Figure S7)

$$i_{p,IV} = -2.576 \times 10^{-5} C_{Tyr} - 8.771 \times 10^{-8}, \quad R^2 = 0.956$$

where $i_{p,IV}$ is the peak IV current density, C_{Tyr} is the concentration of L-Tyr (mM), and R is the correlation coefficient. The scan rate influences for L-Tyr are shown in Figures S7 and S8. All the peak current densities toward $\nu^{1/2}$ exhibited a nearly linear variation, which suggests a mass-transfer process.[40] All the values were calculated according to the methods from previous reports.[41]

Differential Pulse Voltammetry Behavior Studies. Differential pulse voltammetry (DPV) methods have low background current densities and high sensitivity. Compared to the traditional CV methods, they are more suitable for investigating signal-to-background characteristics. In this study, the current response values for the different concentrations of L-Tyr in 1 mM KCl containing 0.1 mM $[Fe(SCN)_6]^{4-/3-}$ solution were studied by DPV methods, as shown in Figure 5a.

As shown in Figure 5a, when adding a small dose of L-Tyr, reduction peak IV at 0.91 V can still be clearly detected. Three reduction peaks can be observed: reduction peak III ($E_{p,III}$ = 0.176 V) belonging to the $[Fe(SCN)_6]^{4-/3-}$ system, reduction peak V ($E_{p,v}$ = 0.64 V) belonging to the electrode-modified material **Cu-1**, and the strong reduction peak IV, which changes significantly with the increase of L-Tyr concentration. The DPV plots (Figure S8) indicated that the peak current density response enhances with the increase of the L-Tyr concentration. It exhibits an excellent linear relationship in the L-Tyr concentration range of 0.01−0.09 mM. The linear variation equation was given as below

$$i_{p,IV} = -2.112 \times 10^{-5} C_{Tyr} + 2.814 \times 10^{-7}, \quad R^2 = 0.998$$

The detection limit (LOD) of L-Tyr was calculated as 5.822 μM by $3\sigma/M$ (n = 10). This study is compared with other previous research studies about L-Tyr detection based on other sensor materials,[42−46] and the relevant parameters of these reports are listed in Table 1. It shows that the **Cu-1** sensor has advantages such as easier preparation and lower production cost. Compared with other widely used materials,[47] the LOD value of the **Cu-1** sensor is close and it can meet the daily test requirements; furthermore, it also has advantages such as easier preparation, lower production cost, and simpler post-treatment.

Table 1. Comparison of Different Detection Methods in the Recognition Efficiency of L-Tyr

electrode materials	detection range	detection limit	ref
TyOx/MWCNT/PSF/GCE	1.96−394 μM	0.3 nM	42
tyrosinase/carbon nanotubes	10−110 μM	2.54 μM	43
poly-L-asp/GPE	0.1−93.9 μM	0.31 μM	44
MIP/RGO composite	0.1−400 μM	0.046 μM	45
graphene-nanowall/Ta film	3−200 μM	0.6 μM	46
Cu-MOF/GCE	0.01−0.09 mM	5.822 μM	this work

Selectivity and Interference Studies. The interference studies from other amino acids, such as D-methionine (D-Met), L-histidine (L-His), L-serine (L-Ser), L-valine (L-Val), L-leucine (L-Leu), L-methionine (L-Met), L-phenylalanine (L-Phe), D-cysteine (D-Cys), L-cysteine (L-Cys), and L-alnine (L-Ala), were also performed. CV methods were used to detect the interferent solution containing 0.5 mM L-Tyr alone or mixed with one or several kinds of these species on the **Cu-1** sensor (Figure 5b, red bars). Reduction peak IV at the potential of 0.91 V can still be observed, and the peak current density value

https://dx.doi.org/10.1021/acs.langmuir.0c02799
Langmuir XXXX, XXX, XXX−XXX

almost did not descend. Subsequently, the selectivity tests were performed by CV for adding 0.1 mM of one type of these species (Figure 5b, blank bars). No other obvious detecting peak can been found. It indicated that the existence of these interferents has few influences for L-Tyr detecting signals. **Cu-1**/GCE has an outstanding selectivity toward L-Tyr.

CONCLUSIONS

In summary, a water-stable 1D double-chain MOF **Cu-1**: $\{[Cu(bpe)(fdc)(H_2O)\ (DMF)]\cdot 0.5H_2O\}_n$ (bpe = 1,2-di(4-pyridyl)ethylene, H_2fdc = 2,5-furandicarboxylic acid) was synthesized by a hydrothermal method. Because of its excellent solvent and electrochemical stability, **Cu-1** without post-treatment was easily used to construct an electrochemical biosensor for efficiently recognizing L-Tyr in a biomimic environment. On comparison with the previous works, it is found that this Cu-MOF sensor possessed good selectivity based on the naked activity sites and an ordered skeleton structure of MOFs which easily form a valid match toward the analyte. A linear range of 0.01−0.09 mmol·L^{-1} for L-Tyr was obtained with an LOD value of 5.822 μM. It shows a promising platform of MOFs to expand their applications in the sensor fields.

ASSOCIATED CONTENT

Supporting Information

The Supporting Information is available free of charge at https://pubs.acs.org/doi/10.1021/acs.langmuir.0c02799.

Single-crystal data, PXRD, TGA, elemental analysis (EA), IR, experimental details, and electrochemical data (PDF)

AUTHOR INFORMATION

Corresponding Author

Xiao-Qin Wu − *Scientific Instrument Center, Shanxi University, Taiyuan 030006, China; Key Laboratory of Advanced Energy Materials Chemistry (Ministry of Education), Nankai University, Tianjin 300071, China;* orcid.org/0000-0002-4230-6644; Email: wxq_1014@sxu.edu.cn

Authors

Pei-Qi Feng − *Scientific Instrument Center, Shanxi University, Taiyuan 030006, China*

Zhiqiang Guo − *Scientific Instrument Center, Shanxi University, Taiyuan 030006, China;* orcid.org/0000-0001-5444-7455

Xuehong Wei − *Scientific Instrument Center, Shanxi University, Taiyuan 030006, China;* orcid.org/0000-0002-9490-7265

Complete contact information is available at: https://pubs.acs.org/10.1021/acs.langmuir.0c02799

Notes

The authors declare no competing financial interest.

ACKNOWLEDGMENTS

We acknowledge Shanxi Key Laboratory of Functional Molecules, who supported this work. Financial support from the Key Laboratory of Advanced Energy Materials Chemistry (Ministry of Education, 111 project, B12015) and the Natural Science Foundation of Shanxi Province (201801D121041) is gratefully acknowledged.

REFERENCES

(1) Savitz, J. The kynurenine pathway: a finger in every pie. *Mol. Psychiatr.* **2020**, *25*, 131−147.

(2) El Ibrahimi, B.; Jmiai, A.; Bazzi, L.; El Issami, S. Amino acids and their derivatives as corrosion inhibitors for metals and alloys. *Arabian J. Chem.* **2020**, *13*, 740−771.

(3) Calendar, R. d-Tyrosyl-tRNA Deacylase: A New Function. *Trends Biochem. Sci.* **2017**, *42*, 684−686.

(4) Li, S.; Liu, J.; Ramesar, N. S.; Heinz, H.; Xu, C.; Kotov, N. A. Single- and multi-component chiral supraparticles as modular enantioselective catalysts. *Nat. Commun.* **2019**, *10*, 4826.

(5) Chen, M.; Wei, J.; Xie, S.; Tao, X.; Zhang, Z.; Ran, P.; Li, X. Bacterial biofilm destruction by size/surface charge-adaptive micelles. *Nanoscale* **2019**, *11*, 1410−1422.

(6) Kumar, M.; Ing, N. L.; Narang, V.; Wijerathne, N. K.; Hochbaum, A. I.; Ulijn, R. V. Amino-acid-encoded biocatalytic self-assembly enables the formation of transient conducting nanostructures. *Nat. Chem.* **2018**, *10*, 696−703.

(7) Jia, R.; Yang, D.; Xu, D.; Gu, T. Mitigation of a nitrate reducing Pseudomonas aeruginosa biofilm and anaerobic biocorrosion using ciprofloxacin enhanced by D-tyrosine. *Sci. Rep.* **2017**, *7*, 6946.

(8) Yan, X.; Li, H.; Jin, R.; Zhao, X.; Liu, F.; Lu, G. Sensitive sensing of enzyme-regulated biocatalytic reactions using gold nanoclusters-melanin-like polymer nanosystem. *Sens. Actuators, B* **2019**, *279*, 281−288.

(9) Hou, J.; Dong, J.; Zhu, H.; Teng, X.; Ai, S.; Mang, M. A simple and sensitive fluorescent sensor for methyl parathion based on l-tyrosine methyl ester functionalized carbon dots. *Biosens. Bioelectron.* **2015**, *68*, 20−26.

(10) Pollock, G. E.; Kawauchi, A. H. Resolution of racemic aspartic acid, tryptophan, hydroxy and sulfhydryl amino acids by gas chromatography. *Anal. Chem.* **1968**, *40*, 1356−1358.

(11) Li, Y.; Pang, T.; Li, Y.; Wang, X.; Li, Q.; Lu, X.; Xu, G. Gas chromatography-mass spectrometric method for metabolic profiling of tobacco leaves. *J. Sep. Sci.* **2011**, *34*, 1447−1454.

(12) Zhu, Q.; Liu, C.; Zhou, L.; Wu, L.; Bian, K.; Zeng, J.; Wang, J.; Feng, Z.; Yin, Y.; Cao, Z. Highly sensitive determination of L-tyrosine in pig serum based on ultrathin CuS nanosheets composite electrode. *Biosens. Bioelectron.* **2019**, *140*, 111356.

(13) Ieda, N.; Nakagawa, H.; Peng, T.; Yang, D.; Suzuki, T.; Miyata, N. Photocontrollable Peroxynitrite Generator Based on N-Methyl-N-nitrosoaminophenol for Cellular Application. *J. Am. Chem. Soc.* **2012**, *134*, 2563−2568.

(14) Tang, X.; Liu, Y.; Hou, H.; You, T. Electrochemical determination of L-Tryptophan, L-Tyrosine and L-Cysteine using electrospun carbon nanofibers modified electrode. *Talanta* **2010**, *80*, 2182−2186.

(15) Zribi, R.; Maalej, R.; Messina, E.; Gillibert, R.; Donato, M. G.; Maragò, O. M.; Gucciardi, P. G.; Leonardi, S. G.; Neri, G. Exfoliated 2D-MoS2 nanosheets on carbon and gold screen printed electrodes for enzyme-free electrochemical sensing of tyrosine. *Sens. Actuators, B* **2020**, *303*, 127229.

(16) Dong, Y.; Li, J.; Zhang, L. 3D hierarchical hollow microrod via in-situ growth 2D SnS nanoplates on MOF derived Co, N co-doped carbon rod for electrochemical sensing. *Sens. Actuators, B* **2020**, *303*, 127208.

(17) Paolesse, R.; Nardis, S.; Monti, D.; Stefanelli, M.; Di Natale, C. Porphyrinoids for Chemical Sensor Applications. *Chem. Rev.* **2017**, *117*, 2517−2583.

(18) Yücebaş, B. B.; Yaman, Y. T.; Bolat, G.; Özgür, E.; Uzun, L.; Abaci, S. Molecular imprinted polymer based electrochemical sensor for selective detection of paraben. *Sens. Actuators, B* **2020**, *305*, 127368.

(19) Meyyappan, M. Carbon Nanotube-Based Chemical Sensors. *Small* **2016**, *12*, 2118−2129.

https://dx.doi.org/10.1021/acs.langmuir.0c02799
Langmuir XXXX, XXX, XXX−XXX

(20) Schroeder, V.; Savagatrup, S.; He, M.; Lin, S.; Swager, T. M. Carbon Nanotube Chemical Sensors. *Chem. Rev.* **2019**, *119*, 599−663.
(21) Singh, E.; Meyyappan, M.; Nalwa, H. S. Flexible Graphene-Based Wearable Gas and Chemical Sensors. *ACS Appl. Mater. Interfaces* **2017**, *9*, 34544−34586.
(22) Skotadis, E.; Mousadakos, D.; Katsabrokou, K.; Stathopoulos, S.; Tsoukalas, D. Flexible polyimide chemical sensors using platinum nanoparticles. *Sens. Actuators, B* **2013**, *189*, 106−112.
(23) Chu, Z.; Peng, J.; Jin, W. Advanced nanomaterial inks for screen-printed chemical sensors. *Sens. Actuators, B* **2017**, *243*, 919−926.
(24) Dong, X.; Yan, X.; Li, M.; Liu, H.; Li, J.; Wang, L.; Wang, K.; Lu, X.; Wang, S.; He, B. Ultrasensitive detection of chloramphenicol using electrochemical aptamer sensor: A mini review. *Electrochem. Commun.* **2020**, *120*, 106835.
(25) Krishnan, S. K.; Singh, E.; Singh, P.; Meyyappan, M.; Nalwa, H. S. A review on graphene-based nanocomposites for electrochemical and fluorescent biosensors. *RSC Adv.* **2019**, *9*, 8778−8881.
(26) Chen, D.-M.; Zhang, X.-J. Stepwise and hysteretic sorption of CO_2 in polycatenated metal−organic frameworks. *CrystEngComm* **2019**, *21*, 4696−4700.
(27) Yi, F.-Y.; Chen, D.; Wu, M.-K.; Han, L.; Jiang, H.-L. Chemical Sensors Based on Metal-Organic Frameworks. *ChemPlusChem* **2016**, *81*, 675−690.
(28) Zhu, C.; Gerald, R. E.; Chen, Y.; Huang, J. Metal-organic framework portable chemical sensor. *Sens. Actuators, B* **2020**, *321*, 128608.
(29) Yu, H.; Zhang, W.; Lv, S.; Han, J.; Xie, G.; Chen, S. A one-step structure-switching electrochemical sensor for transcription factor detection enhanced with synergistic catalysis of PtNi@MIL-101 and Exo III-assisted cycling amplification. *Chem. Commun.* **2018**, *54*, 11901−11904.
(30) Wang, J.; Zhao, J.; Yang, J.; Cheng, J.; Tan, Y.; Feng, H.; Li, Y.; Acta, M. An electrochemical sensor based on MOF-derived NiO@ZnO hollow microspheres for isoniazid determination. *Mikrochim. Acta* **2020**, *187*, 380.
(31) Ye, Z.; Wang, Q.; Qiao, J.; Xu, Y.; Li, G. In situ synthesis of sandwich MOFs on reduced graphene oxide for electrochemical sensing of dihydroxybenzene isomers. *Analyst* **2019**, *144*, 2120−2129.
(32) Song, Y.; Xu, M.; Gong, C.; Shen, Y.; Wang, L.; Xie, Y.; Wang, L. Ratiometric electrochemical glucose biosensor based on GOD/AuNPs/Cu-BTC MOFs/macroporous carbon integrated electrode. *Sens. Actuators, B* **2018**, *257*, 792−799.
(33) Zhao, X.; Bai, J.; Bo, X.; Guo, L. A novel electrochemical sensor based on 2D CuTCPP nanosheets and platelet ordered mesoporous carbon composites for hydroxylamine and chlorogenic acid. *Chim. Acta* **2019**, *1075*, 71−80.
(34) Meng, Z.; Stolz, R. M.; Mendecki, L.; Mirica, K. A. Electrically-Transduced Chemical Sensors Based on Two-Dimensional Nanomaterials. *Chem. Rev.* **2019**, *119*, 478−598.
(35) Ciucci, F. Modeling electrochemical impedance spectroscopy. *Curr. Opin. Electrochem.* **2019**, *13*, 132−139.
(36) Blair, E. O.; Corrigan, D. K. A review of microfabricated electrochemical biosensors for DNA detection. *Biosens. Bioelectron.* **2019**, *134*, 57−67.
(37) Laviron, E. General expression of the linear potential sweep voltammogram in the case of diffusionless electrochemical system. *J. Electroanal. Chem.* **1979**, *101*, 19−28.
(38) Borcherding, N.; Kusner, D.; Liu, G.-H.; Zhang, W. ROR1, an embryonic protein with an emerging role in cancer biology. *Protein Cell* **2014**, *5*, 496−502.
(39) Yang, Y.; Song, Y.; Bo, X.; Min, J.; Pak, O. S.; Zhu, L.; Wang, M.; Tu, J.; Kogan, A.; Zhang, H.; Hsiai, T. K.; Li, Z.; Gao, W. A laser-engraved wearable sensor for sensitive detection of uric acid and tyrosine in sweat. *Nat. Biotechnol.* **2020**, *38*, 217−224.
(40) Wu, X.-Q.; Liu, Y.; Feng, P.-Q.; Wei, X.-H.; Yang, G.-M.; Qiu, X.-H.; Ma, J.-G. Design of a Zn-MOF Biosensor via a Ligand "Lock" for the Recognition and Distinction of S-containing Amino Acids. *Chem. Commun.* **2019**, *55*, 4059−4062.
(41) Gabriels, R. General Method for Calculating the Detection Limit in Chemical Analysis. *Anal. Chem.* **1970**, *42*, 1439−1440.
(42) Phelane, L.; Gouveia-Caridade, C.; Barsan, M. M.; Baker, P. G. L.; Brett, C. M. A.; Iwuoha, E. I. Electrochemical Determination of Tyrosine using a Novel Tyrosinase Multi-Walled Carbon Nanotube (MWCNT) Polysulfone Modified Glassy Carbon Electrode (GCE). *Anal. Lett.* **2020**, *53*, 308.
(43) Apetrei, C.; Apetrei, I. M. Biosensor based on tyrosinase immobilized on a single-walled carbon nanotube-modified glassy carbon electrode for detection of epinephrine. *Int. J. Nanomed.* **2013**, *8*, 4391−4398.
(44) Luo, Y.; Zhang, Y.; Lu, L.; Luo, H. A flexible CVD graphene platform electrode modified with L -aspartic acid for the simultaneous determination of acetaminophen, epinephrine and tyrosine. *J. Electroanal. Chem.* **2020**, *856*, 113737.
(45) Zheng, W.; Zhao, M.; Liu, W.; Yu, S.; Niu, L.; Li, G.; Li, H.; Liu, W. Electrochemical sensor based on molecularly imprinted polymer/reduced graphene oxide composite for simultaneous determination of uric acid and tyrosine. *J. Electroanal. Chem.* **2018**, *813*, 75−82.
(46) Tian, F.; Li, H.; Li, M.; Li, C.; Lei, Y.; Yang, B. A tantalum electrode coated with graphene nanowalls for simultaneous voltammetric determination of dopamine, uric acid, L-tyrosine, and hydrochlorothiazide. *Microchim. Acta* **2017**, *184*, 1611−1619.
(47) Kochana, J.; Hnida, K.; Sulka, G.; Knihnicki, P.; Kozak, J.; Gilowska, A. Application of polypyrrole nanowires for the development of a tyrosinase biosensor. *Chem. Pap.* **2015**, *69*, 1130−1135.

https://dx.doi.org/10.1021/acs.langmuir.0c02799
Langmuir XXXX, XXX, XXX−XXX